

# Phase ordering with a global conservation law: Ostwald ripening and coalescence

Massimo Conti<sup>1</sup>, Baruch Meerson<sup>2</sup>, Avner Peleg<sup>2</sup> and Pavel V. Sasorov<sup>3</sup>

<sup>1</sup> *Dipartimento di Matematica e Fisica, Università di Camerino,*

*and Istituto Nazionale di Fisica della Materia, 62032, Camerino, Italy*

<sup>2</sup> *The Racah Institute of Physics, The Hebrew University of Jerusalem, Jerusalem 91904, Israel*

<sup>3</sup> *Institute for Theoretical and Experimental Physics, Moscow, 117259, Russia*

Globally conserved phase ordering dynamics is investigated in systems with short range correlations at  $t = 0$ . A Ginzburg-Landau equation with a global conservation law is employed as the phase field model. The conditions are found under which the sharp-interface limit of this equation is reducible to the area-preserving motion by curvature. Numerical simulations show that, for both critical and off-critical quench, the equal time pair correlation function exhibits dynamic scaling, and the characteristic coarsening length obeys  $l(t) \sim t^{1/2}$ . For the critical quench, our results are in excellent agreement with earlier results. For off-critical quench (Ostwald ripening) we investigate the dynamics of the size distribution function of the minority phase domains. The simulations show that, at large times, this distribution function has a self-similar form with growth exponent  $1/2$ . The scaled distribution, however, strongly differs from the classical Wagner distribution. We attribute this difference to coalescence of domains. A new theory of Ostwald ripening is developed that takes into account binary coalescence events. The theoretical scaled distribution function agrees well with that obtained in the simulations.

## I. INTRODUCTION

Phase ordering is emergence of order from disorder through domain growth and coarsening. The standard setting when phase ordering occurs is a temperature quench from a high-temperature disordered phase into a two-phase or a multiphase region. Phase ordering has been the subject of extensive research during the last two decades [1]. An important simplifying assumption in phase ordering theory is dynamic scale invariance. According to this assumption, the coarsening system possesses, at late times, a single relevant dynamic length scale  $l(t)$  (the characteristic domain size) which grows with time as  $l(t) \sim t^\alpha$  [1]. It is by now well established that in systems with short range correlations  $\alpha = 1/2$  for non-conserved (model A) dynamics, while  $\alpha = 1/3$  for locally conserved (model B) dynamics.

There is, however, an important additional coarsening mechanism: *globally conserved* phase ordering [2, 3, 4, 5, 6, 7]. Globally conserved dynamics can be thought of as model A dynamics constrained by global conservation of the order parameter: for example, Ising model with fixed magnetization. This global conservation law is maintained by an external field (for example, a magnetic field) which depends on time but is uniform in space. The globally-conserved phase ordering is accessible in experiment. Consider the sublimation/deposition dynamics of a solid and its vapor in a small closed vessel kept at a constant temperature below the melting point. As the acoustic time scale in the gas phase is short compared to the coarsening time, the gas pressure (and, consequently, density) remain uniform in space, changing only in time. This character of mass transport in the vapor phase makes the coarsening dynamics conserved globally rather than locally. An important characteristics of globally-conserved dynamics is interface-controlled kinetics, in contrast to the bulk-diffusion-controlled kinetics typical for locally-conserved systems. Interface-controlled kinetics was investigated in the context of growth of small platinum particles supported on alumina substrates in an oxidizing environment [8]. There are additional examples of cluster growth on surfaces [9], where it was found possible to single out the interface-controlled kinetics [10]. There is also strong evidence in favor of globally conserved interface-controlled transport during the coarsening of clusters in granular powders driven by a low-frequency electric field [11, 12].

Part of the theoretical importance of globally conserved phase ordering lies in the fact that it enables an access to off-critical quenches in the simpler model A dynamics (with global conservation). Thus, it allows one to determine which characteristics of the system depend on the volume (or area) fraction  $\varepsilon$  and which do not.

Dynamic renormalization group arguments show that global conservation should not change the growth law [13]. This early result was confirmed by particle simulations with short range correlations in the initial conditions: for critical ( $\varepsilon = 1/2$ ) [6, 14] and for off-critical ( $\varepsilon < 1/2$ ) [4] quench. Recent phase field simulations of systems with long-range (power-law) correlations in the initial conditions have also shown dynamic scale invariance with the same growth exponent  $\alpha = 1/2$  [7]. Therefore,  $\alpha = 1/2$  independently of  $\varepsilon$ . On the other hand, the autocorrelation function [4, 15] and persistence exponent [15] were found to be  $\varepsilon$ -dependent.

Globally conserved dynamics are related to a wide range of multiphase coarsening systems. Sire and Majumdar [4] showed that in the large- $q$  limit the dynamics of the  $q$ -state Potts model are equivalent to the dynamics of the globally conserved model with an area fraction  $\varepsilon = 1/q$ . The large- $q$  limit of the Potts model is of practical importance as it describes correctly some of the dynamic characteristics of dry soap froths [16] and of the coarsening of polycrystalline

materials [17].

In the limit of a vanishing volume fraction of the minority phase the late stage of coarsening is describable by the mean field theories of Ostwald ripening. Lifshitz and Slyozov [18] developed such a theory for the bulk-diffusion-controlled (or locally conserved) dynamics. They showed that the size distribution function of the minority domains approaches, at large times, a self-similar form. Correspondingly, the average size of the minority phase domains grows with time like  $t^{1/3}$ . Following the seminal work by Lifshitz and Slyozov [18], Wagner developed a similar mean-field theory for the interface-controlled (globally conserved) Ostwald ripening [19]. The Wagner's theory yields a growth law  $t^{1/2}$  for the average domain size, and a different (broader) shape of the scaled distribution function. We shall refer to this scaled distribution function as the Wagner distribution. More recently, it was shown that interface-controlled Ostwald ripening appears in the sharp-interface limit of scalar Ginzburg-Landau equations (and its modifications) with a global conservation law [2, 3, 4, 5, 20].

Although the simple theories of Lifshitz-Slyozov and Wagner were developed more than 40 years ago, they are still very useful in phase ordering theory. For example, Sire and Majumdar [4] employed the Wagner distribution to calculate the equal-time pair correlation function. Lee and Rutenberg [15] used the two theories of Ostwald ripening for calculating the autocorrelation exponent and persistence exponent for the locally- and globally-conserved systems.

Many works were devoted to extensions of the Lifshitz-Slyozov theory to finite volume fractions. Already Lifshitz and Slyozov [18] made an attempt to go beyond their simple model and account for coalescence. Later it became clear that, in the locally-conserved systems, the dominant effect unaccounted for by the simple theory is inter-domain correlations, rather than coalescence. At small area fractions, the relative role of correlations is of order  $\varepsilon^{1/2}$  [21], while the relative role of coalescence is of order  $\varepsilon$ . Therefore, an account of coalescence without a proper account of correlations is an excess of accuracy.

The situation is quite different in globally-conserved systems, and this fact has not been recognized until now. Correlations between neighboring domains are *exponentially* small in this case [3, 5]. Therefore, coalescence is expected to give the dominant correction to the theory of Wagner [19]. We shall report numerical simulations that show a strong effect of coalescence at moderate  $\varepsilon$ . Specifically, we find that, at large times, the size distribution function of the minority domains has a self-similar form with the "normal" growth exponent 1/2. The scaled distribution function, however, strongly differs from the Wagner distribution. We attribute this difference to coalescence and develop a new theory of Ostwald ripening that takes coalescence into account.

The outline of the rest of the paper is the following. In Section II we briefly review the phase field model of globally conserved phase ordering: a scalar Ginzburg-Landau equation with a global conservation law. The sharp-interface asymptotic limit of this equation is introduced and reduced, in 2D, to a simpler model of area-preserving motion by curvature. The criteria for the validity of this reduction are obtained and presented in Appendix. The model of area-preserving motion by curvature is used to obtain dynamic scaling laws for the characteristic coarsening length and for the effective magnetic field. The results of the phase field simulations for the critical quench ( $\varepsilon = 0.50$ ) and off-critical quench ( $\varepsilon = 0.25$ ) are presented and analyzed in Section III. In Section IV a new theory of Ostwald ripening is developed. The theory leads to a non-linear integro-differential equation for the scaled distribution function. The solution of this equation is in good agreement with the scaled size distribution function found in the phase field simulations. In Section V we summarize our results.

## II. PHASE FIELD MODEL AND SHARP-INTERFACE LIMIT

Globally conserved phase ordering dynamics are describable by a simple phase field model [3, 4, 6]. In this model the free energy functional has the Ginzburg-Landau form:

$$F[u] = \int \left[ \frac{\delta}{2\mu} (\nabla u)^2 + V(u) + Hu \right] d^d \mathbf{r}, \quad (1)$$

and the dynamics follow a simple gradient descent:

$$\partial_t u = -\mu \frac{\delta F}{\delta u} = \delta \nabla^2 u + \mu (u - u^3 - H(t)). \quad (2)$$

Either no-flux or periodic boundary conditions can be used. In Eqs. (1) and (2)  $u(\mathbf{r}, t)$  is the coarse-grained order parameter field,  $V(u) = (1/4)(1 - u^2)^2$  is a symmetric double-well potential,  $\delta$  is the diffusion coefficient,  $\mu$  is the characteristic rate of relaxation of the field  $u$  to its stable equilibrium values, and  $d$  is the dimension of space. The effective uniform magnetic field  $H(t)$  changes in time so as to impose the global conservation law:

$$\langle u(\mathbf{r}, t) \rangle = L^{-d} \int u(\mathbf{r}, t) d^d \mathbf{r} = \text{const}, \quad (3)$$

where  $L$  is the system size and the integration is carried out over the entire system. Integrating both sides of Eq. (2) over the entire system and using Eq. (3) and the boundary conditions we obtain:

$$H(t) = \langle u - u^3 \rangle = L^{-d} \int [u(\mathbf{r}, t) - u^3(\mathbf{r}, t)] d^d \mathbf{r}. \quad (4)$$

Therefore, Eq. (2) takes the form:

$$\partial_t u = \delta \nabla^2 u + \mu(u - u^3) - \mu \langle u - u^3 \rangle, \quad (5)$$

a globally-constrained Ginzburg-Landau equation (GLE). From now on we shall concentrate on the 2D case.

At late stages of the coarsening process, the system consists of domains of "phase 1" (where  $u$  is close to  $-1$ ) and "phase 2" (where  $u$  is close to  $1$ ) separated by domain walls. The domain walls can be treated as sharp interfaces [5, 22], as their characteristic width  $\lambda = (\delta/\mu)^{1/2}$  is much smaller than the characteristic domain size  $l(t)$  which grows with time. At this stage  $H(t)$  is already small,  $H(t) \ll 1$ , and slowly varying in time. The phase field in the phases 1 and 2 is almost uniform and rapidly adjusting to the value of  $H(t)$ , so  $u \simeq -1 - H(t)/2$  and  $u \simeq 1 - H(t)/2$  in the phases 1 and 2, respectively. Under these conditions, the so called "sharp-interface theory" holds. The normal velocity of the interface  $v_n$  is given by [5]:

$$v_n(s, t) = \delta \kappa(s, t) + (\delta \mu)^{1/2} g H(t), \quad (6)$$

where  $s$  is a coordinate along the interface,  $\kappa(s, t)$  is the local curvature, and  $g = -3/\sqrt{2}$ . A positive  $v_n$  corresponds to the interface moving towards phase 1, while a positive  $\kappa$  corresponds to an interface which is convex towards phase 2. The dynamics of  $H(t)$  are described by [5]:

$$\dot{H}(t) = \frac{4\Lambda(t)}{L^2} \left[ \overline{\delta \kappa(s, t)} + (\delta \mu)^{1/2} g H(t) \right]. \quad (7)$$

Here  $\overline{\kappa(s, t)}$  is the interface curvature averaged over the whole interface:

$$\overline{\kappa(s, t)} = \frac{1}{\Lambda(t)} \oint \kappa(s, t) ds, \quad (8)$$

and  $\Lambda(t) = \oint ds$  is the total perimeter of the interface. Equations (6) and (7) provide a general sharp-interface formulation for the GLE with a global conservation law.

Let us denote by  $A(t)$  the total area of phase 2:

$$A(t) = \int_{u(\mathbf{r}, t) > 0} d^2 \mathbf{r}.$$

Equations (6) and (7) can be used to calculate the rate of change of  $A(t)$ :

$$\dot{A}(t) = \oint v_n(s, t) ds = \Lambda(t) \left[ \overline{\delta \kappa(s, t)} + (\delta \mu)^{1/2} g H(t) \right]. \quad (9)$$

Using Eqs. (7) and (9) we obtain:  $\dot{H} = 4\dot{A}/L^2$  which yields the global conservation law:

$$A(t) - \frac{L^2 H(t)}{4} = \text{const}. \quad (10)$$

The second term in Eq. (10) corresponds to the bulk order parameter  $u$  being biased by  $H(t)$ . One can use Eq. (10) instead of Eq. (7) in the general sharp-interface formulation of the problem.

In some important cases this formulation can be simplified further [5, 7, 23]. When the two terms on the right hand side of Eq. (9) approximately balance each other,

$$H(t) \simeq -\frac{1}{g} \left( \frac{\delta}{\mu} \right)^{1/2} \overline{\kappa(s, t)}, \quad (11)$$

the area of each of the two phases remains constant. In this case Eq. (6) takes the form:

$$v_n(s, t) = \delta \left[ \kappa(s, t) - \overline{\kappa(s, t)} \right]. \quad (12)$$

Dynamics (12) are known as area-preserving motion by curvature in 2D, and as volume-preserving motion by mean curvature in 3D [3, 5, 24]. Due to the presence of the non-local term  $\bar{\kappa}$  this model is different from the Allen-Cahn equation [25]  $v_n = \delta \kappa$ , which represents the sharp-interface limit for non-conserved (model A) dynamics [1].

A simple example where the area-preserving dynamics *cannot* be used is the dynamics of a single circular domain of the minority phase in a “sea” of the majority phase [5, 20]. Another example is the dynamics of a “donut”: a single domain of the minority phase with an inclusion of a majority phase domain [26]. Therefore, the first question we need to address concerns the general conditions under which the area-preserving dynamics, Eq. (12), represent an accurate approximation to the more general sharp-interface theory, Eqs. (6) and (7). These conditions are derived in Appendix.

Now we employ the area-preserving model and do simple dynamic scaling analysis. (In the rest of the paper we are using dimensionless variables and put  $\delta = \mu = 1$ .) For critical quench we have  $H(t) = 0$  and  $\overline{k(s,t)} = 0$  because of symmetry between the two phases (we neglect finite-size effects). Therefore, the globally conserved dynamics for critical quench are *identical* to the non-conserved (model A) dynamics. Using the Allen-Cahn equation  $v_n(s,t) = \kappa(s,t)$ , one arrives at the well-known scaling law  $l(t) \sim t^{1/2}$  [1].

Turning to the off-critical quench, we notice that, under the scaling assumption, the interface velocity can be estimated as  $v_n \sim dl/dt$ . Each of the two terms on the right hand side of Eq. (12) is of order  $1/l(t)$ . Equating and integrating, we again obtain  $l(t) \sim t^{1/2}$ . Therefore, global conservation does not change the dynamic scaling for *any* area fraction. This result was previously obtained by dynamic renormalization group arguments applied to Eq. (5) (with a Gaussian white noise term) [13], and by particle simulations [4]. For the off-critical dynamics of  $H(t)$  we have:  $|H(t)| = |\langle \kappa(s,t) \rangle / g| \sim 1/l(t) \sim t^{-1/2}$ .

Though the dynamic exponent is independent of the area fraction, other characteristics can depend on it. In the following Section we report numerical simulations that address area-fraction-dependent quantities.

### III. NUMERICAL SIMULATIONS

We performed extensive simulations by directly solving Eq. (5) with initial conditions in the form of “white noise”. The simulations were done for two different values of the area fraction of the minority phase:  $\varepsilon = 0.50$ , and  $\varepsilon = 0.25$ , corresponding to a critical and off-critical quench, respectively. In both cases the results were averaged over 10 different samples. Eq. (5) was discretized and solved on a  $1024 \times 1024$  domain, with mesh size  $\Delta x = \Delta y = 1$  and periodic boundary conditions. The coarsening process was followed up to a time  $t = 3000$ . An explicit Euler integration scheme was used to advance the solution in time, and the Laplace operator was discretized by second order central differences. A time step  $\Delta t = 0.1$  was required for numerical stability. The accuracy of the numerical scheme was monitored by checking the (approximate) conservation law (10) of the general sharp-interface theory. It was found that this conservation law is obeyed with an accuracy better than 0.02% for  $t > 4$  and better than 0.008% for  $t > 30$  in the critical quench case. In the off-critical quench the approximate conservation law (10) is obeyed with an accuracy better than 1% for  $t > 30$ . To avoid any misunderstanding here and in the following we notice that, in all cases, the *integrated order parameter* [see Eq. (3)] is conserved exactly by the numerical scheme.

It is convenient to introduce an auxiliary density field  $\rho(\mathbf{r}, t) = (1/2)[u(\mathbf{r}, t) + 1]$ . The minority phase is identified as the locus where  $\rho(\mathbf{r}, t) \geq 1/2$ . Typical snapshots of the coarsening process are shown in Fig. 1 for the critical quench, and in Fig. 2 for the off-critical quench. For the critical quench the system consists of interpenetrating domains of the two phases. For the off-critical quench the morphology is that of Ostwald ripening [27]: larger domains of the minority phase grow at the expense of smaller ones. As the minority phase area fraction is not very small, binary (and even triple) coalescence events are clearly seen in Fig. 2. Overall, the coarsening morphologies resemble those observed for locally-conserved system: in numerical solutions of the Cahn-Hilliard equation [28] and in particle simulations [29]. An important difference is an apparent absence of correlations between neighboring domains in Fig. 2.

To analyze the coarsening dynamics, the following quantities were sampled and averaged over the 10 initial conditions:

1. The area of phase 2.
2. The circularly averaged equal-time pair correlation function:

$$C(r, t) = \frac{\langle \rho(\mathbf{r}', t) \rho(\mathbf{r}' + \mathbf{r}, t) \rangle - \langle \rho(\mathbf{r}', t) \rangle^2}{\langle \rho^2(\mathbf{r}', t) \rangle - \langle \rho(\mathbf{r}', t) \rangle^2}. \quad (13)$$

3. The characteristic coarsening length scale  $l(t)$ , determined from the condition  $C(l, t) = 1/2$ .
4. The effective magnetic field  $H(t)$  computed from Eq. (4).

5. The size distribution function of the minority phase domains (for the off-critical quench).

For critical quench we found that the area of the minority phase is constant with an accuracy better than 0.03% at all times. The situation is quite different for the off-critical quench. Here there is a systematic trend in the area fraction of the minority phase. Still, with time this quantity approaches a constant value. Deviations from this constant value become less than 3% for  $t > 100$ . This approximate area conservation plays a crucial role in the theory of Ostwald ripening (see Sec. IV).

Figure 3 shows, on a single graph, the scaling forms of the correlation function  $C(x)$ , where  $x = r/l(t)$ , for the critical and off-critical quench. The  $l(t)$ -dependence is presented in Fig. 4. A comparison of the scaling forms  $C(x)$  with those obtained in particle simulations of globally conserved [6] and non-conserved [30] dynamics for critical quench is also shown. The three curves for the critical quench almost coincide. For off-critical quench, the  $C(x)$  curve is slightly different from the curves for the critical quench. A similar weak dependence of the scaled correlation function on the area fraction of the minority phase was observed in locally conserved systems [28, 29, 31].

Figure 4 shows corrected power-law fits  $l(t) = l_0 + bt^\alpha$  which yield  $\alpha = 0.50$ ,  $l_0 = 0.5$ , and  $b = 1.2$  for the critical quench, and  $\alpha = 0.51$ ,  $l_0 = 1.3$ , and  $b = 0.9$  for the off-critical quench. A pure  $t^{1/2}$  power-law line serves as a reference for the expected late-time dynamic behavior. Therefore,  $l(t)$  obeys the expected  $t^{1/2}$  dynamical scaling law, in agreement with the predictions of the dynamic renormalization group analysis [13] and area-preserving sharp-interface theory. The difference in the values of the amplitudes  $b$  again indicates a dependence on the minority phase area fraction.

The time history of  $1/|H(t)|$  for the off-critical quench is presented in Fig. 5. The data is fitted by a corrected power-law:  $1/|H(t)| = a + ct^\alpha$  with  $a = 7.4$ ,  $c = 2.3$ , and  $\alpha = 0.51$ . Also shown is a  $2.3t^{1/2}$  power law, serving as a reference to the expected late-time dynamics. We conclude that  $|H(t)| \sim t^{-1/2}$ , as predicted by the sharp-interface theory. The significance of the value of the amplitude  $c$  will be discussed in Section IV in the context of our theory of Ostwald ripening with coalescence. One can distinguish in Fig. 5 small "fluctuations" of  $1/|H(t)|$  around a smooth trend. (This is in contrast to the  $l(t)$ -dependence where no fluctuations are observed.) To interpret these fluctuations we use Eqs. (11) and (50) to obtain:  $1/|H(t)| \sim \Lambda(t)/N_2(t)$ .  $\Lambda(t)$  is a continuous function of  $t$ , whereas  $N_2(t)$  behaves discontinuously at the time moments when domains disappear due to shrinking and merging events. Thus  $H(t)$  serves as a "domain counter".

For critical quench,  $H(t)$  exhibits very small irregular fluctuations around zero. The typical values of  $H(t)$  in this case are of the order of  $10^{-5}$ , and we interpret these fluctuations as finite-size effects.

As we have shown, the scaled correlation function only weakly depends on the area fraction. A much more sensitive diagnostics of the off-critical quench dynamics is provided by the size distribution function of the minority phase domains. We found that, at late times, this function exhibits dynamic scaling. Figure 6 shows the scaled form  $\Phi_{num}$  of the distribution function obtained in the simulations with the GLE. The scaled variable on the horizontal axis of Fig. 6 is  $\xi = R/t^{1/2}$ , where the effective radius of each domain is defined as  $R = (A_d/\pi)^{1/2}$  and  $A_d$  is the domain area. Function  $\Phi_{num}$  was obtained, at each moment of time, by multiplying the values of the distribution function, found in the simulations, by  $t^{3/2}$ . The dynamic exponents  $1/2$  and  $3/2$  are the same as in the classical theory of Wagner [19].

Here is a more detailed account of our calculation of the scaled distribution function. We chose for sampling 13 time moments in the interval  $120 < t < 2900$ . The domain statistics is obviously better at earlier times of this interval, and it deteriorates at later times, as many domains shrink and disappear. On the other hand, the dynamic exponent  $1/2$  shows up, with a good accuracy, only at relatively late times (see Figs. 4 and 5). Therefore, we had to include the relatively late times in our sampling, which led to relatively big error bars in Fig. 6.

The area fraction  $\varepsilon = 0.25$ , used in our simulations, is moderately large. Therefore, one could expect significant deviations of the scaled distribution function, found numerically, from the Wagner distribution [19] corresponding to the same area fraction (that is, having the same second moment). The Wagner distribution has the following form:

$$\Phi_W(\xi) = C \varepsilon \frac{\xi}{(\xi - \sqrt{2})^4} \exp\left(-\frac{2\sqrt{2}}{\sqrt{2} - \xi}\right) \quad (14)$$

for  $\xi < \sqrt{2}$ , and  $\Phi_W(\xi) = 0$  for  $\xi \geq \sqrt{2}$ . The normalization constant

$$C = \frac{1}{\pi [(2e^2)^{-1} + Ei(-2)]} \simeq 16.961,$$

where  $Ei(\dots)$  is the exponential integral function [32].

The two distributions,  $\Phi_{num}(\xi)$  and  $\Phi_W(\xi)$ , are shown in the same Fig. 6. One can see that the difference between them is enormous (in order to show the Wagner distribution on the same graph with  $\Phi_{num}$ , we had to multiply it by a factor of 0.5). Therefore, at moderate area fractions, the Wagner's theory is inapplicable.

It is instructive to compare the zero moments  $M_0$  of the two distributions. The zero moment is the amplitude of the scaling law for the number density of domains at large times:  $n(t) = M_0 t^{-1}$ . We obtained  $M_0 = 4.72 \cdot 10^{-2}$  for  $\Phi_{num}$  and  $M_0 \simeq 1.43 \cdot 10^{-1}$  for  $\Phi_W$ . Therefore, for  $\varepsilon = 0.25$  the Wagner distribution overestimates the number of domains at late times by a factor of 3. An additional difference is the pronounced tail in  $\Phi_{num}$  which extends much further than the edge of the compact support of the Wagner distribution. Coalescence provides a natural explanation to these two facts: coalescence events reduce the total number of domains and produce domains of progressively larger size. We shall see in the next Section that an account of coalescence leads to a good quantitative agreement between theory and simulations.

#### IV. THEORY OF OSTWALD RIPENING WITH COALESCENCE

In this Section we present a new theory of the globally-conserved (interface-controlled) Ostwald ripening that accounts for coalescence. One of our assumptions is that each domain can be represented by an equivalent *circular* domain, or droplet, the area of which is equal to the area of the domain. We shall denote by  $f(R, t)$  the distribution function of the droplets with respect to their radii.  $f(R, t)$  is normalized by the condition  $\int_0^\infty f(R, t) dR = n(t)$ , where  $n(t)$  is the number density of the droplets. We start with a brief review of the ‘‘classical’’ theory that neglects coalescence and goes back to Wagner [19]. Then we derive a kinetic equation that accounts of coalescence. We shall focus on the long-time, self-similar asymptotic solutions to that kinetic equation, find the solution by an iteration procedure and compare it with the result of the phase-field simulations.

##### A. Ostwald ripening without coalescence: a brief review

At a late stage of coarsening  $|H(t)| \ll 1$ , so there is no nucleation of new domains. Then, neglecting coalescence, one can write a simple continuity equation in  $R$ -space for the size distribution function of domains, or droplets:

$$\partial_t f + \partial_R (\dot{R} f) = 0. \quad (15)$$

When criterion (51) is satisfied, the dynamics are describable by the area-preserving motion by curvature (12) (where we put  $\delta = 1$ ). This leads immediately to

$$\dot{R} = \frac{1}{R_c(t)} - \frac{1}{R}, \quad (16)$$

where the time-dependent critical radius  $R_c(t) = \sqrt{2}/(3|H(t)|)$  is determined, at a late stage of coarsening, by the conservation of the total area of the minority phase:

$$\pi \int_0^\infty R^2 f dR = \varepsilon = const. \quad (17)$$

Equations (15)-(17) represent the classical model of interface-controlled Ostwald ripening. This model was formulated by Wagner [19] by analogy with the theory of Lifshitz and Slyozov [18] developed for the locally conserved (diffusion-controlled) dynamics. Using Eqs. (15)-(17), one obtains

$$R_c(t) = \frac{\int_0^\infty R f dR}{\int_0^\infty f dR} = \langle R(t) \rangle, \quad (18)$$

where  $\langle R(t) \rangle$  is the time-dependent average radius of the droplets.

Droplets with  $R > R_c(t)$  grow at the expense of droplets with  $R < R_c(t)$  which shrink. The late-time asymptotic behavior described by Eqs. (15)-(17) is the following [19]. The critical radius grows with time (this corresponds to the decrease with time of the effective magnetic field which plays the role of supersaturation). As a result, a droplet which was growing at an early time begins to shrink at a later time. Since all the quantities are position-independent, this model represents a mean-field theory. It should be noticed that the mean-field approximation is much more accurate for the globally-conserved (interface-controlled) Ostwald ripening than for the locally-conserved (diffusion-controlled) Ostwald ripening [5]. First, in the globally-conserved case, the ‘‘mean field’’  $H(t)$  is the actual field in the system. This is in contrast to the diffusion-controlled Ostwald ripening [18], where a mean field description of the supersaturation is an approximation valid only when the typical distances between the droplets are very large compared to the typical droplet radius. The second difference concerns the role of correlations. In the locally-conserved case, correlations

between droplets result from the Laplacian screening effect, and their relative contribution to the size distribution function is of order  $\varepsilon^{1/2}$  (see, *e.g.* Ref. [21]). The effect of coalescence scales like  $\varepsilon$  (see below) so, at small  $\varepsilon$ , correlation effects should be much less significant. By contrast, in the interface-controlled case direct correlations between droplets are exponentially small, and significant correlations can be caused only by coalescence events. Therefore, in the interface-controlled case, it is legitimate to account for coalescence while neglecting correlations.

Wagner [19] obtained a self-similar solution to Eqs. (15)-(17) (the Wagner distribution) that corresponds to a long-time asymptotics of the initial-value problem. The similarity Ansatz is

$$f(R, t) = \frac{1}{t^{3/2}} \Psi_\beta \left( \frac{R}{t^{1/2}} \right), \quad R_c(t) = \frac{t^{1/2}}{\beta}, \quad (19)$$

where  $\beta$  is a constant number. The scaled distribution  $\Psi_\beta(\xi)$  obeys an ordinary differential equation:

$$\left( -\frac{\xi}{2} + \beta - \frac{1}{\xi} \right) \Psi'_\beta(\xi) + \left( -\frac{3}{2} + \frac{1}{\xi^2} \right) \Psi_\beta(\xi) = 0. \quad (20)$$

The total area conservation (17) leads to normalization condition

$$\pi \int_0^\infty \xi^2 \Psi_\beta(\xi) d\xi = \varepsilon = \text{const}. \quad (21)$$

Formally solving Eq. (20), one actually obtains a *family* of solutions parameterized by  $\beta$ . For  $\sqrt{2} \leq \beta \leq 2\sqrt{2/3}$  these solutions have compact support: they are positive on an interval  $0 < \xi < \xi_{max}(\beta)$ , and zero elsewhere. Similar solutions in 3D were investigated in Refs. [5, 20, 33]. We call these solutions *localized*. For  $0 < \beta < \sqrt{2}$  the solutions of Eq. (20) are extended: they have an infinite tail. These solutions can be written as  $\text{const} \cdot \Psi_{0\beta}(\xi)$ , where

$$\Psi_{0\beta}(\xi) = \frac{\xi}{(\xi^2 - 2\beta\xi + 2)^2} \times \exp \left( -\frac{2\beta}{\sqrt{2 - \beta^2}} \arctan \frac{\xi - \beta}{\sqrt{2 - \beta^2}} \right). \quad (22)$$

Extended solutions fall off like  $\xi^{-3}$  as  $\xi \rightarrow \infty$ . As a result, the integral in Eq. (21) diverges logarithmically, so the extended solutions are non-normalizable. Still, as we shall see, they play a crucial role in the theory of Ostwald ripening with coalescence.

Which of the similarity solutions is selected by the dynamics (that is, represents a long-time asymptotics of the initial value problem)? It turns out that selection is “weak”, that is, determined by the initial conditions. The Wagner distribution is selected for (normalizable) *extended* initial distributions. On the contrary, if the initial distribution  $f(R, t = 0)$  has compact support, one of the *localized* distributions is selected. The selection is determined by the asymptotics of  $f(R, t = 0)$  near the upper edge of its support [5, 20, 33].

However, this weak selection rule was obtained in the framework of the classical formulation of the problem, Eqs. (15)-(17). One can expect that *strong* selection (independent of the initial conditions) can be obtained if one goes beyond the classical formulation. Indeed, it was shown in Ref. [34] (see also [35]) that an account of fluctuations leads to strong selection. Fluctuations produce a tail in the time-dependent distribution function and drive the solution towards the Wagner distribution. We shall see in the following that an account of coalescence also leads to strong selection, even in the absence of fluctuations.

## B. Kinetic equation with coalescence

We shall now take into account the processes of binary coalescence. Coalescence events occur when two droplets contact each other. Within the framework of the GLE, the positions of the droplet centers remain fixed. Therefore, for coalescence to happen, at least one of the droplets must be expanding. Consider a droplet of radius  $R_1 < R < R_1 + \Delta R_1$ . The number density of such droplets is  $f(R_1, t)\Delta R_1$ . Now consider another droplet of radius  $R_2 < R < R_2 + \Delta R_2$  in the vicinity of the first droplet. If  $\dot{R}_1 + \dot{R}_2 > 0$  then, during the time interval  $\Delta t$ , the distance between the boundaries of these droplets will decrease by  $(\dot{R}_1 + \dot{R}_2)\Delta t$ . If the distance  $r$  between the centers of the droplets obeys the double inequality

$$(R_1 + R_2) \leq r \leq (R_1 + R_2) + (\dot{R}_1 + \dot{R}_2)\Delta t, \quad (23)$$

(which assumes that the condition  $\dot{R}_1 + \dot{R}_2 > 0$  is fulfilled), then these two droplets will collide during the time interval  $\Delta t$ . Therefore, for the two droplets to collide, the center of the second droplet should be located within a circular ring, concentric with the first droplet, with radius  $R_1 + R_2$  and width  $(\dot{R}_1 + \dot{R}_2)\Delta t$ . The area of this ring is equal to

$$2\pi(R_1 + R_2)(\dot{R}_1 + \dot{R}_2)\Delta t. \quad (24)$$

Hence, the average number of such second droplets is equal to

$$2M(R_1, R_2)f(R_2, t)\Delta R_2\Delta t,$$

where

$$M(R_1, R_2) = \pi(R_1 + R_2)(\dot{R}_1 + \dot{R}_2)\theta(\dot{R}_1 + \dot{R}_2).$$

The total number of the collision events per unit area is equal to

$$[2M(R_1, R_2)f(R_2, t)\Delta R_2\Delta t]f(R_1, t)\Delta R_1. \quad (25)$$

Each collision leads to coalescence: disappearance of a droplet of radius  $R_1$  and a droplet of radius  $R_2$ , and creation of a new droplet.

Now we make two assumptions that will enable us to construct a closed theory. First, we assume that the area of a new droplet, formed by a binary coalescence event, is equal to the sum of the areas of the two merging droplets. Second, we assume that new droplet *instantaneously* becomes circular [36], so its radius is  $(R_1^2 + R_2^2)^{1/2}$ . The kinetic equation for the size distribution function includes the rates of gains and losses of droplets by coalescence. This leads to the following equation:

$$\begin{aligned} \partial_t f + \partial_R(\dot{R}f) = & -\frac{1}{2} \int_0^\infty \int_0^\infty \{2M(R_1, R_2) \times \\ & \left[ \delta(R - R_1) + \delta(R - R_2) - \delta\left(R - \sqrt{R_1^2 + R_2^2}\right) \right] \times \\ & f(R_1, t) f(R_2, t) dR_1 dR_2\}, \end{aligned} \quad (26)$$

where  $\delta(\dots)$  is the Dirac's delta-function and the factor 1/2 is introduced in order to avoid counting each coalescence event twice. Performing integration with  $\delta(R - R_1)$  and  $\delta(R - R_2)$  and taking into account the symmetry of  $M(R_1, R_2)$  under a transposition of its arguments:

$$M(R_1, R_2) = M(R_2, R_1),$$

we obtain:

$$\begin{aligned} \partial_t f + \partial_R(\dot{R}f) = & \\ = & -2f(R, t) \int_0^\infty M(R, R_1)f(R_1, t) dR_1 + \\ & + \int_0^\infty \int_0^\infty M(R_1, R_2) \delta\left(R - \sqrt{R_1^2 + R_2^2}\right) \times \\ & f(R_1, t) f(R_2, t) dR_1 dR_2. \end{aligned} \quad (27)$$

Integration of the right hand side of Eq. (27) over  $R^2 dR$  yields zero, so the new kinetic equation preserves the conservation law (17) as it should. In addition, the simple relation (18) continues to hold. Integrating the right



hand side of Eq. (27) over  $dR$ , and over  $RdR$ , respectively, one can show that the coalescence term reduces the number density of the droplets and the total interface length. Moreover, the new equation preserves the dynamic scaling. Indeed, if some  $f(R, t)$  and  $R_c(t)$  give a solution to Eqs. (27), (17) and (18), then  $f'(R, t) = \eta^3 f(\eta R, \eta^2 t)$  and  $R'_c(t) = \eta^{-1} R_c(\eta^2 t)$  give another solution to the same equations. This invariance under a stretching transformation implies the existence of a self-similar solution that will be considered in the next subsection.

While deriving Eq. (27), we neglected effects of interactions of three droplets. By this we refer to cases where there are three closely lying droplets. In these cases triple coalescence events may occur. In addition, an excluded area in the ring (23) appears. The effects of this excluded area, and of the triple coalescence events were not taken into account in our theory. These effects are expected to be of order  $\varepsilon^3$ , while the effects of binary coalescence events are of order  $\varepsilon^2$ . Therefore, Eq. (27) is expected to be valid for small area fractions  $\varepsilon$ . We shall see, however, that a very good accuracy is obtained even for the moderate value of  $\varepsilon = 0.25$  used in our simulations, when triple coalescence events do occur (see Fig. 2).

Another limitation of our theory concerns the large- $R$  tail of  $f(R, t)$ . The tail shape is affected by higher-order coalescence events unaccounted for in our theory. This limitation is not very important in practice. The main contribution to the critical radius  $R_c$  comes, for normalizable distributions, by the “body” of the distribution function, rather than by the tail.

We conclude this subsection by a brief discussion of a different type of coalescence: Brownian coalescence. Following the pioneering work of Smoluchowski [37], Binder and Stauffer [38] suggested a mean-field scenario of phase separation in alloys in which clusters of the minority phase are regarded as Brownian particles: they perform random walk in space. When two clusters collide, they merge into a larger single cluster. The corresponding kinetic equation includes an integral term whose general structure resembles that of the integral term in Eq. (27), but with a different kernel  $M(R_1, R_2)$ . If the cluster diffusivity is a power-law function of the cluster size, one arrives at a self-similar solution for the size distribution function of the droplets. An important further development was the work of Siggia [39] who considered hydrodynamic interactions between randomly moving and coalescing droplets in phase separating binary fluids. Following the work of Siggia, the Brownian coalescence in binary fluids has been extensively studied theoretically and experimentally. Among important issues here is a crossover from Ostwald ripening (the Lifshitz-Slyozov-Wagner mechanism) to Brownian coalescence [1, 39, 40], plethora of hydrodynamic interactions in the process of coalescence [39, 41, 42], scaling violations [43] etc. In parallel, Brownian coalescence has been investigated in the context of coarsening of clusters of atoms or vacancies diffusing on surfaces, following particle deposition [44]. It is clear that Brownian coalescence is different in its nature from the coalescence process considered in this work. In contrast to Brownian coalescence, droplets in our system do not move: they coalesce only because they grow.

### C. Self-similar solution with coalescence

Equations (27) and (17) admit the same similarity Ansatz as Eqs. (15) and (17):

$$f(R, t) = \frac{1}{t^{3/2}} \Phi \left( \frac{R}{t^{1/2}} \right) \quad (28)$$

and

$$R_c(t) = \beta^{-1} t^{1/2}, \quad (29)$$

where  $\beta$  is again an unknown yet constant number. The scaled distribution function  $\Phi(\xi)$  obeys the following integro-differential equation:

$$\begin{aligned} & \left( -\frac{\xi}{2} + \beta - \frac{1}{\xi} \right) \Phi'(\xi) + \left( -\frac{3}{2} + \frac{1}{\xi^2} \right) \Phi(\xi) = \\ & -2\Phi(\xi) \int_0^\infty w(\xi, \xi_1) \Phi(\xi_1) d\xi_1 + \\ & \int_0^\infty \int_0^\infty w(\xi_1, \xi_2) \delta \left( \xi - \sqrt{\xi_1^2 + \xi_2^2} \right) \Phi(\xi_1) \Phi(\xi_2) d\xi_1 d\xi_2 \end{aligned} \quad (30)$$

subject to normalization condition

$$\pi \int_0^\infty \xi^2 \Phi(\xi) d\xi = \varepsilon. \quad (31)$$

In Eq. (30) we denoted

$$w(\xi_1, \xi_2) = \pi (\xi_1 + \xi_2) \left( 2\beta - \frac{1}{\xi_1} - \frac{1}{\xi_2} \right) \times \\ \theta \left( 2\beta - \frac{1}{\xi_1} - \frac{1}{\xi_2} \right), \quad (32)$$

where  $\theta(\dots)$  is the theta-function. It is convenient to rewrite Eq. (30) in a symbolic form:

$$\mathcal{L}_\beta \Phi = \mathcal{N}_\beta[\Phi], \quad (33)$$

where

$$\mathcal{L}_\beta \Phi(\xi) = \left( -\frac{\xi}{2} + \beta - \frac{1}{\xi} \right) \Phi'(\xi) + \left( -\frac{3}{2} + \frac{1}{\xi^2} \right) \Phi(\xi), \quad (34)$$

and

$$\mathcal{N}_\beta[\Phi](\xi) = -2\Phi(\xi) \int_0^\infty w(\xi, \xi_1) \Phi(\xi_1) d\xi_1 + \\ \int_0^\infty \int_0^\infty w(\xi_1, \xi_2) \delta \left( \xi - \sqrt{\xi_1^2 + \xi_2^2} \right) \Phi(\xi_1) \Phi(\xi_2) d\xi_1 d\xi_2. \quad (35)$$

One important property of Eq. (30) can be noticed immediately: the coalescence term vanishes identically at  $0 \leq \xi < 1/(2\beta)$ . As a result, the scaled distribution function at  $0 \leq \xi < 1/(2\beta)$  should coincide (up to a  $\xi$ -independent multiplier) with one of the solutions of the classical Wagner's problem. A simple argument shows that parameter  $\beta$ , parameterizing this solution, should be less than  $\sqrt{2}$ . Indeed, inverting the linear operator  $\mathcal{L}_\beta$ , we rewrite Eq. (33) as an integral (rather than integro-differential) equation:

$$\Phi(\xi) = \Psi_\beta(\xi) \left[ \int_\xi^\infty \frac{\mathcal{N}_\beta[\Phi(\xi')]}{\left( \frac{\xi'}{2} - \beta + \frac{1}{\xi'} \right) \Psi_\beta(\xi')} d\xi' + C_1 \right], \quad (36)$$

where functions  $\Psi_\beta(\xi)$  were introduced in subsection A and  $C_1$  is a constant. Unless  $\beta < \sqrt{2}$ , the integral over  $d\xi'$  diverges. Therefore,  $\Psi_\beta(\xi)$  should be one of the *extended* solutions  $\Psi_{0\beta}(\xi)$ , given by Eq. (22). In addition, since the second term in the square brackets of Eq. (36) would lead to divergence of the integral appearing in the normalization condition (31), we must choose  $C_1 = 0$ . Hence, Eq. (36) reads:

$$\Phi(\xi) = \Psi_{0\beta}(\xi) \int_\xi^\infty \frac{\mathcal{N}_\beta[\Phi(\xi')]}{\left( \frac{\xi'}{2} - \beta + \frac{1}{\xi'} \right) \Psi_{0\beta}(\xi')} d\xi'. \quad (37)$$

Integral equation (37) and normalization condition (31) make a complete set. For a given  $\varepsilon$ , the scaled distribution function  $\Phi = \Phi_\beta(\xi)$  and parameter  $\beta = \beta(\varepsilon)$  are uniquely determined. Therefore, an account of coalescence does provide strong selection to the problem of Ostwald ripening.

#### D. Solving Eqs. (37) and (31)

Our procedure for solving Eqs. (37) and (31) employs the one-to-one correspondence between  $\varepsilon$  and  $\beta$ . Therefore, one can fix  $\beta$  and solve Eq. (37) by iterations for  $\Phi = \Phi_\beta(\xi)$ . The normalization condition (31) is *not* used at this stage. After a sufficiently accurate estimate for  $\Phi = \Phi_\beta(\xi)$  is obtained, one employs Eq. (31) to calculate  $\varepsilon$  that corresponds to this  $\beta$ . Repeating this procedure for different  $\beta$ , one obtains the family of solutions  $\Phi_\beta(\xi)$  and the dependence  $\varepsilon = \varepsilon(\beta)$ . Inverting this dependence, one arrives at  $\beta = \beta(\varepsilon)$  and finds the correspondence between  $\varepsilon$  and scaled distributions  $\Phi_\beta(\xi) = \Phi_{\beta(\varepsilon)}(\xi)$ .

Now we introduce an iteration scheme that implements this idea. The scheme exploits the fact that, for the exact solution of Eq. (37),

$$\Phi(\xi) = \chi \Psi_{0\beta}(\xi) \quad \text{at} \quad 0 \leq \xi < \frac{1}{2\beta}, \quad (38)$$

where  $\chi = \chi(\beta)$  is  $\xi$ -independent and unknown in advance. Let us introduce an auxiliary unknown function  $\phi(\xi) = \chi^{-1}\Phi(\xi)$  [45]. By definition,

$$\phi(\xi) = \Psi_{0\beta}(\xi) \quad \text{at} \quad 0 \leq \xi < \frac{1}{2\beta}. \quad (39)$$

In terms of the new function  $\phi$ , Eq. (37) becomes

$$\phi(\xi) = \chi \Psi_{0\beta}(\xi) \int_{\xi}^{\infty} \frac{\mathcal{N}_\beta[\phi(\xi')] d\xi'}{\left(\frac{\xi'}{2} - \beta + \frac{1}{\xi'}\right) \Psi_{0\beta}(\xi')}. \quad (40)$$

The iteration scheme for Eq. (40) is the following:

$$\begin{aligned} \phi_{k+1}(\xi) = \\ \chi_k \Psi_{0\beta}(\xi) \int_{\xi}^{\infty} \frac{\mathcal{N}_\beta[\phi_k(\xi')] d\xi'}{\left(\frac{\xi'}{2} - \beta + \frac{1}{\xi'}\right) \Psi_{0\beta}(\xi')}, \end{aligned} \quad (41)$$

for  $k = 0, 1, 2, \dots$ . We use the arbitrariness of  $\chi_k$  and demand that, at each iteration, Eq. (39) is satisfied:

$$\phi_{k+1}(\xi) = \Psi_{0\beta}(\xi) \quad \text{at} \quad 0 \leq \xi < \frac{1}{2\beta}. \quad (42)$$

This implies

$$\chi_k = \left[ \int_{1/(2\beta)}^{\infty} \frac{\mathcal{N}_\beta[\phi_k(\xi)] d\xi}{\left(\frac{\xi}{2} - \beta + \frac{1}{\xi}\right) \Psi_{0\beta}(\xi)} \right]^{-1}, \quad (43)$$

for  $k = 0, 1, 2, \dots$ . Equation (43) and (41) define the iteration process explicitly. If the sequence  $\phi_k$ ,  $k = 0, 1, 2, \dots$  converges to a finite limit  $\phi(\xi)$ , then the sequence  $\chi_k$ ,  $k = 0, 1, 2, \dots$  converges to a finite (positive) number  $\chi$ , and we can find  $\Phi(\xi) = \chi \phi(\xi)$ . What is left is to use Eq. (31) and compute the corresponding  $\varepsilon$ . If the convergence of the iteration scheme is fast enough, then

$$\Phi_k(\xi) = \chi_k \phi_k(\xi) \quad (44)$$

and

$$\varepsilon_k(\beta) = \pi \chi_k \int \xi^2 \phi_k(\xi) d\xi, \quad k = 1, 2, \dots \quad (45)$$

give a good approximation to the solution already after a small number of iterations.

We implemented this iteration procedure numerically. As it is clear from Eqs. (41), (43), (44) and (45), the numerics involve only calculations of (double and triple) definite integrals. We started with the trial function  $\phi_0(\xi) = \Psi_{0\beta}(\xi)$ .

The advantage of this trial function is that it already satisfies Eq. (39). We performed a detailed investigation of the convergence of this scheme for different values of  $\beta$  up to iteration  $k = 8$ . The results of this investigation (and proofs of convergence of the integrals at infinity) will be presented in a separate publication. The main result is that, with this choice of the trial function, the convergence is very fast in the body of the scaled distribution function. For example, in the case of  $\varepsilon = 0.25$  the first iteration already gives an accurate result. Convergence in the tail is a more subtle issue that will be addressed separately.

The  $\beta(\varepsilon)$ -dependence, found by this procedure is shown in Fig. 7. One can see that, as  $\varepsilon \rightarrow 0$ ,  $\beta \rightarrow \sqrt{2}$  from below. Overall, this behavior is expected. Coalescence effects become small at small area fractions and, as  $\varepsilon \rightarrow 0$ , the scaled distribution function should approach the Wagner distribution. It is surprising, however, that for quite small  $\varepsilon$  (for example, 0.01), the value of  $\beta$  is still significantly different from  $\sqrt{2}$ .

Figure 6 shows the scaled distribution function for  $\beta = 0.93$  (which corresponds to  $\varepsilon \simeq 0.25$ ). The solid line shows the result of the first iteration  $\Phi_1(\xi)$ . This result agrees well with the phase field simulations, even at the moderately large value of  $\varepsilon = 0.25$ . This is a strong evidence in favor of the major role of coalescence in the interface-controlled Ostwald ripening. The dashed line is the trial function  $\Phi_0(\xi)$ . One can see that this trial function (with  $\beta = 0.93$ ) already gives a fairly accurate estimate to the solution in the body of the scaled distribution. Therefore, the non-normalizable extended distributions (22) do play a special role in the theory. In the tail region the solution falls off more rapidly than  $\Psi_{0\beta}$ , so there is no problem with normalization condition (31). The zero moment  $M_0$  corresponding to the once-iterated numerical solution (the solid line in Fig. 6) is equal to  $5.08 \cdot 10^{-2}$  which is in good agreement with the value  $4.72 \cdot 10^{-2}$  obtained in the simulations.

An independent estimate of  $\beta$  at  $\varepsilon = 0.25$  is provided by the dynamics of the effective "magnetic field"  $H(t)$ . The area-preserving dynamics, Eq. (12), imply that  $|H(t)| \simeq |\sqrt{2}\bar{\kappa}/3|$ . Assuming that all droplets have circular shape (an assumption already used in our theory), we have  $|\kappa| = 1/\langle R(t) \rangle$ . Employing the similarity solution, we arrive at  $|\kappa| = \beta/t^{1/2}$ . Therefore,  $1/|H(t)| \sim c t^{1/2}$ , where  $c = 3/(\sqrt{2}\beta)$ . For the corrected power-law fit shown in Fig. 5  $c = 2.3$ . This corresponds to  $\beta \simeq 0.92$  which is remarkably close to the value of 0.93 obtained by the iteration procedure.

## V. CONCLUSIONS

We investigated globally conserved phase ordering dynamics in systems with short range correlations. The numerical simulations were done with a 2D phase-field model: a Ginzburg-Landau equation with a global conservation law. The sharp-interface limit of this equation: the area-preserving motion by curvature was introduced, and a criterion for its validity formulated. Assuming dynamic scaling within the model of area-preserving motion by curvature, we obtained the  $1/2$  dynamic exponent for the characteristic coarsening length scale (for critical and off-critical quench), and for the effective "magnetic field" (for off-critical quench). Our numerical simulations for critical quench and for an off-critical quench with area fraction  $\varepsilon = 0.25$  confirm these scaling laws. The results for critical quench coincide with earlier results, obtained by particle simulations. The scaled form of the equal-time pair-correlation function is found to weakly depend on the area fraction, similar to the locally-conserved systems.

Recently, dynamic scale invariance and "normal" scaling have been reported in the same globally conserved coarsening system, but for *long-range* (power-law) correlations in the initial conditions [7]. Our present results, combined with those of Ref. [7], indicate "normal" scaling properties of globally conserved systems for any generic initial conditions.

The main focus of this work was on the dynamics of the size distribution function of the minority phase domains for the off-critical quench. Our phase field simulations show that this distribution function exhibits, at large times, a self-similar form. The scaled distribution function, however, is dramatically different from the well-known Wagner distribution, despite the fact that correlations between domains are negligible in globally-conserved systems. We attributed this strong deviation to coalescence that provides, at small  $\varepsilon$ , a leading correction to the Wagner's theory. We developed a new theory of Ostwald ripening that takes into account binary coalescence events. The theory possesses dynamic scale invariance and yields a non-linear integro-differential equation for the scaled distribution function. For a given area fraction, the problem has a unique solution. Therefore, coalescence renders a strong selection rule to the problem of Ostwald ripening: the scaled distribution is selected by the area fraction of the minority domains. The scaled distribution function predicted by the new theory is in good agreement with the scaled distribution obtained from the phase field simulations for a moderate area fraction of 0.25. In addition, the new theory accurately predicts the amplitude of the late-time power law of the effective magnetic field  $H(t)$ . Deviations from the classical Wagner's theory remain significant even for very low area fractions. Therefore, coalescence plays a major role in the interface-controlled Ostwald ripening.

We hope that the results of this work will stimulate further experiments on globally-conserved interface-controlled systems.

### Acknowledgments

We are grateful to B.P. Vollmayr-Lee for useful discussions. This work was supported in part by the Israel Science Foundation, administered by the Israel Academy of Sciences and Humanities, and by the Russian Foundation for Basic Research (grant No. 99-01-00123).

### Appendix. Criteria for the area-preserving dynamics

Let us find the general conditions under which the area-preserving dynamics [Eq. (12)] represent an accurate approximation to the more general sharp-interface theory [Eqs. (6) and (7)]. We first notice that in the general sharp-interface theory it is the quantity  $A(t) - L^2 H(t)/4$ , rather than  $A(t)$ , that is conserved [5]. Hence, a necessary condition for the validity of the area-preserving dynamics is simply

$$H(t) \ll \frac{A(t)}{L^2}. \quad (46)$$

Additional criteria are found in the following manner. We notice that Eq. (7) includes the same combination  $\delta\bar{k} + (\delta\mu)^{1/2}gH(t)$  as the one that appears on the right hand side of Eq. (9). Therefore a constancy or, more precisely, slow variation of  $A(t)$  implies a slow variation of  $H(t)$ . Correspondingly, the term on the left hand side of Eq. (7) should be small in this case compared to each of the two terms on the right hand side. We can exploit this fact and formally solve Eq. (7) perturbatively:  $H(t) = H^{(0)}(t) + h(t)$ , where  $H^{(0)}(t) = -g^{-1}(\delta/\mu)^{1/2} \bar{\kappa}$ , is the leading term, and  $h(t)$  is the subleading term. Substituting  $H(t)$  into Eq. (7) and keeping terms up to order  $h(t)$  we obtain:

$$h(t) = \frac{L^2}{4g(\delta\mu)^{1/2}\Lambda(t)} \dot{H}^{(0)}(t) = -\frac{L^2}{4g^2\mu\Lambda(t)} \overline{\dot{\kappa}(s,t)}. \quad (47)$$

The perturbation expansion is valid as long as

$$|h(t)| \ll |H^{(0)}(t)| \quad \text{and} \quad \frac{|h(t)|}{(\delta\mu)^{1/2}\Lambda(t)} \ll \frac{|h(t)|}{L^2}.$$

Using the expressions for  $H^{(0)}(t)$  and  $h(t)$  we see that the dynamics described by (6) and (7) are (approximately) area-preserving if the following two inequalities hold:

$$\frac{|\overline{\dot{\kappa}(s,t)}|}{(\delta\mu)^{1/2}\Lambda(t)} \ll \frac{|\overline{\kappa(s,t)}|}{L^2}, \quad (48)$$

and

$$\left| \frac{d}{dt} \left[ \frac{\overline{\dot{k}(s,t)}}{(\delta\mu)^{1/2}\Lambda(t)} \right] \right| \ll \frac{|\overline{\dot{k}(s,t)}|}{L^2}. \quad (49)$$

Now we can see why the area-preserving dynamics do not apply to a single circular droplet. In this case the zero order of the perturbation theory would give  $\overline{\kappa(s,t)} = 1/R = \text{const}$ , where  $R$  is the droplet radius. Therefore, criterion (48) is violated.

For a ‘‘donut’’ one has  $\overline{\kappa(s,t)} = 0$ . Therefore, neither of the two criteria (48) and (49) is obeyed, and the dynamics are not area-preserving. If the system consists of  $N_1(t)$  domains of the majority phase and  $N_2(t)$  domains of the minority phase, the Gauss-Bonnet theorem [46] yields

$$\overline{\kappa(s,t)} = \frac{2\pi(N_1(t) - N_2(t))}{\Lambda(t)}, \quad (50)$$

where  $N_1(t)$  does not include the large ‘‘sea’’ of the majority phase. We shall employ this relation in the following.

Let us check criteria (46), (48) and (49) for the ‘‘standard problem’’ of phase-ordering, when the initial conditions describe a disordered state with short-ranged correlations. We assume that the system exhibits, at late times, dynamic scale invariance. In other words, the characteristic domain size  $l(t)$  is the only relevant length scale. For an off-critical quench, the phase-ordering morphology is that of Ostwald ripening: competition of droplets of the minority phase, see

below. This implies the following scaling relations:  $\overline{\kappa(s,t)} \sim 1/l(t)$ ,  $\overline{k(s,t)} \sim \delta/l^3(t)$ , and  $\Lambda(t) \sim N_2(t)l(t) \sim \varepsilon L^2/l(t)$ . In addition,  $H(t) \sim \lambda/l(t)$  and  $A = \varepsilon L^2$ . Using these relations in any of the inequalities (46), (48) or (49), we arrive at

$$\frac{\lambda}{l(t)} \ll \varepsilon. \quad (51)$$

That is, the more general sharp-interface theory is reducible to the area-preserving motion by curvature as long as the ratio between the interface width and the coarsening length scale is much smaller than the area fraction of the minority phase. If the coarsening system remains a two-phase system, and if the system size is big enough, this condition holds, at late times, for any nonzero area fraction [47]. Notice that, at  $\varepsilon \ll 1$  it takes more time for the system to reach the area-preserving regime.

- 
- [1] A.J. Bray, *Adv. Phys.* **43**, 357 (1994).  
[2] L. Schimansky-Geier, C. Zülicke and E. Schöll, *Z. Phys. B-Cond. Mat.* **84**, 433 (1991).  
[3] J. Rubinstein and P. Sternberg, *IMA J. Appl. Math.* **48**, 249 (1992).  
[4] C. Sire and S.N. Majumdar, *Phys. Rev. Lett.* **74**, 4321 (1995); *Phys. Rev. E* **52**, 244 (1995).  
[5] B. Meerson and P.V. Sasorov, *Phys. Rev. E* **53**, 3491 (1996).  
[6] A.D. Rutenberg, *Phys. Rev. E* **54**, 972 (1996).  
[7] A. Peleg, M. Conti, and B. Meerson, *Phys. Rev. E* **64**, 036127 (2001).  
[8] P. Wynblatt and N.A. Gjostein, in: *Progress in Solid State Chemistry*, edited by J.O. McCaldin and G. Somojrai, (Pergamon, Oxford, 1975) Vol. 9, p. 21.  
[9] M. Zinke-Allmang, L.C. Feldman, and M.H. Grabow, *Surface Sci. Reports* **16**, 277 (1992).  
[10] Z. Toroczkai and E. Williams, *Phys. Today* **52** (12), 24 (1999).  
[11] I. S. Aranson, D. Blair D, V.A. Kalatsky, G.W. Crabtree, W.K. Kwok, V.M. Vinokur, and U. Welp, *Phys. Rev. Lett.* **84**, 3306 (2000).  
[12] I. Aranson, B. Meerson, P.V. Sasorov and V.M. Vinokur, e-print cond-mat/0107443.  
[13] A.J. Bray, *Phys. Rev. Lett.* **66**, 2048 (1991), and references therein.  
[14] J.F. Annett and J.R. Banavar, *Phys. Rev. Lett.* **68**, 2941 (1992); L.L. Moseley, P.W. Gibbs, and N. Jan, *J. Stat. Phys.* **67**, 813 (1992).  
[15] B.P. Lee and A.D. Rutenberg, *Phys. Rev. Lett.* **79**, 4842 (1997).  
[16] J.A. Glazier, M.P. Anderson, and G.S. Grest, *Philos. Mag. B* **62**, 615 (1990).  
[17] G.S. Grest, M.P. Anderson, and D.J. Srolovitz, *Phys. Rev. B* **38**, 4752 (1988).  
[18] I.M. Lifshitz and V.V. Slyozov, *Zh. Eksp. Teor. Fiz.* **35**, 479 (1958) [*Sov. Phys. JETP* **8**, 331 (1959)]; *J. Phys. Chem. Solids*, **19**, 35 (1961).  
[19] C. Wagner, *Z. Elektrochem.* **65**, 581 (1961).  
[20] I. Aranson, B. Meerson, and P.V. Sasorov, *Phys. Rev. E* **52**, 948 (1995).  
[21] M. Marder, *Phys. Rev. A* **36**, 858 (1987).  
[22] A.S. Mikhailov, *Foundations of Synergetics I. Distributed Active Systems* (Springer-Verlag, Berlin, 1993).  
[23] A. Peleg, B. Meerson, A. Vilenkin, and M. Conti, *Phys. Rev. E* **63**, 066101 (2001).  
[24] M. Gage, *Contemp. Math.* **51**, 51 (1986).  
[25] S.M. Allen and J.W. Cahn, *Acta Metall.* **27**, 1085 (1979).  
[26] B. Meerson and I. Mitkov, *Phys. Rev. E* **54**, 4644 (1996).  
[27] W. Ostwald, *Z. Phys. Chem.* **34**, 495 (1900).  
[28] T.M. Rogers and R.C. Desai, *Phys. Rev. B* **39**, 11956 (1989).  
[29] P. Fratzl, J.L. Lebowitz, O. Penrose, and J. Amar, *Phys. Rev. B* **44**, 4794 (1991).  
[30] K. Humayun and A.J. Bray, *J. Phys. A* **24**, 1915 (1991); *Phys. Rev. B* **46**, 10594 (1992).  
[31] K.R. Elder and R.C. Desai, *Phys. Rev. B* **40**, 243 (1989).  
[32] S. Wolfram, *The Mathematica Book*, 3rd ed. (Cambridge Univ. Press, 1996), p. 1081.  
[33] B. Giron, B. Meerson, and P.V. Sasorov, *Phys. Rev. E* **58**, 4213 (1998).  
[34] B. Meerson, *Phys. Rev. E* **60**, 3072 (1999).  
[35] I. Rubinstein and B. Zaltzman, *Phys. Rev. E* **61**, 709 (2000).  
[36] In fact, new droplets just formed by coalescence do not have a circular form (see Fig. 2). However, for small  $\varepsilon$ , deviations from the circular form are significant for big droplets, that is in the tail of the size distribution function. In the “body” of the size distribution function (which gives the dominant contribution to the critical radius  $R_c$ ), the droplets are already close to circular.  
[37] M. von Smoluchowski, *Z. Phys. Chem.* **92**, 129 (1917).  
[38] K. Binder and D. Stauffer, *Phys. Rev. Lett.* **33**, 1006 (1974).  
[39] E.D. Siggia, *Phys. Rev. A* **20**, 595 (1979).  
[40] C.K. Haas, J.M. Torkelson, *Phys. Rev. E* **55**, 3191 (1997).

- [41] H. Tanaka, J. Chem. Phys. **105**, 10099 (1996).
- [42] V.S. Nikolaev, D. Beysens and P. Guenoun, Phys. Rev. Lett. **76**, 3144 (1996).
- [43] A.J. Wagner and J.M. Yeomans, Phys. Rev. Lett. **80**, 1429 (1998).
- [44] C.R. Stoldt, C.J. Jenks, P.A. Thiel, A.M. Cadilhe and J.W. Evans, J. Chem. Phys. **111**, 5157 (1999); D. Kandel, Phys. Rev. Lett. **79**, 4238 (1997).
- [45] One can check that a straightforward iteration scheme for  $\Phi(\xi)$  would diverge.
- [46] E. Kreyszig, *Differential Geometry* (University of Toronto Press, Toronto, 1959).
- [47] A criterion similar to Eq. (51) also appears when the initial condition represents a single long stripe [23]. In that case  $l(t)$  is the stripe length.

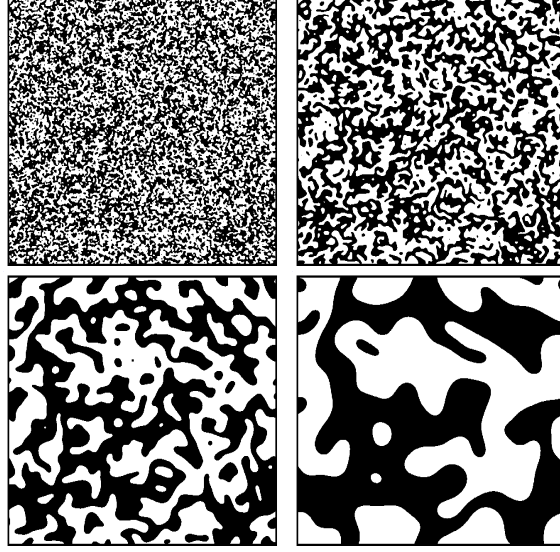


FIG. 1: Snapshots of globally conserved coarsening for critical quench. The upper row corresponds to  $t = 5.2$  (left) and  $32.3$  (right), the lower row to  $t = 204.8$  (left) and  $1305.5$  (right).

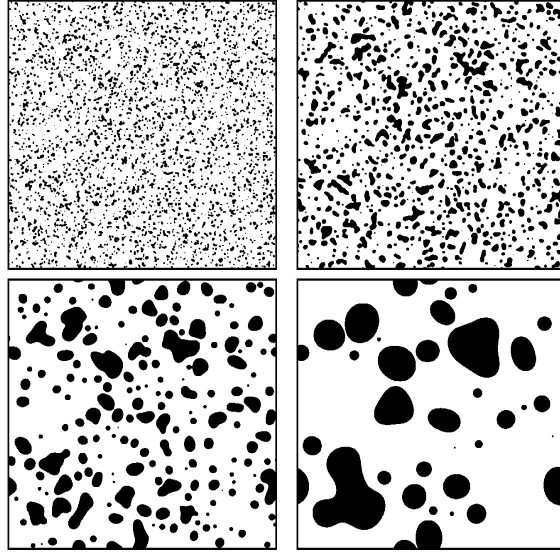


FIG. 2: Snapshots of globally conserved coarsening for off-critical quench with area fraction  $\varepsilon = 0.25$ . The upper row corresponds to  $t = 5.2$  (left) and  $32.3$  (right), the lower row to  $t = 204.8$  (left) and  $1305.5$  (right).



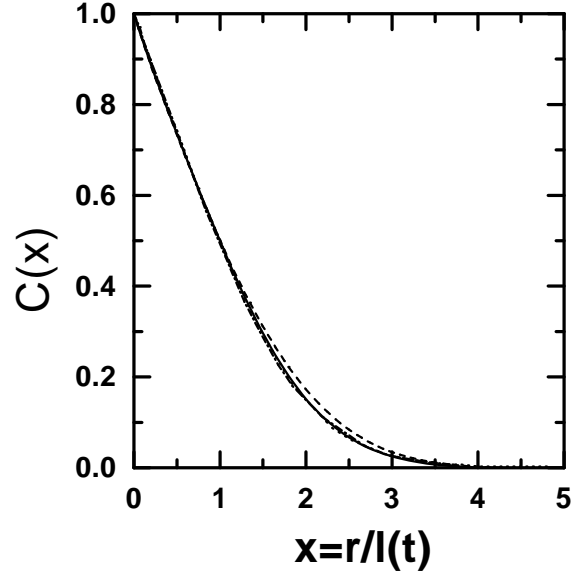


FIG. 3: Scaled correlation function obtained by numerical simulations with the GLE subject to a global conservation law for times  $t > 15$ . The solid line is  $C(x)$  for critical quench, and the dashed line is  $C(x)$  for off-critical quench with area fraction  $\varepsilon = 0.25$ . The dotted (dashed-dotted) line represents  $C(x)$  obtained in particle simulations of globally conserved [6] (non-conserved [30]) dynamics for critical quench.

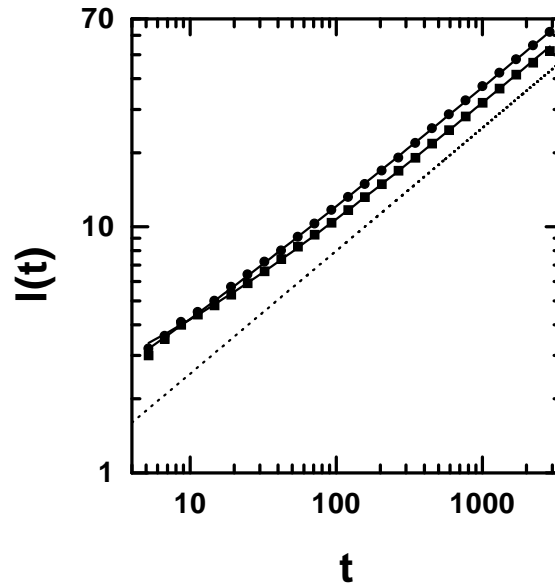


FIG. 4: Characteristic coarsening length  $l$  vs. time for the critical quench (circles), and off-critical quench with area fraction  $\varepsilon = 0.25$  (squares). The two solid lines are corrected power-law fits  $l(t) = l_0 + bt^\alpha$  with  $\alpha = 0.50$ ,  $l_0 = 0.5$ , and  $b = 1.2$  for the critical quench, and  $\alpha = 0.51$ ,  $l_0 = 1.3$ , and  $b = 0.9$  for the off-critical quench. The dotted line shows a pure  $t^{1/2}$  power law.

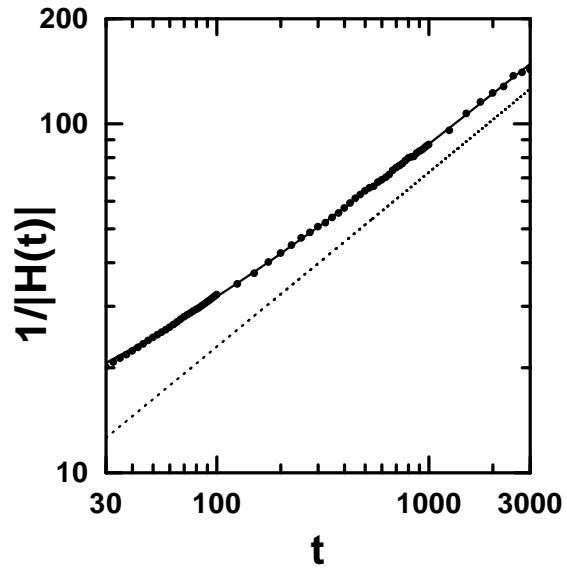


FIG. 5:  $1/|H(t)|$  vs. time for an off-critical quench with area fraction  $\varepsilon = 0.25$  (circles). The solid line is a corrected power law fit  $1/|H(t)| = a + ct^\alpha$  with  $a = 7.4$ ,  $c = 2.3$ , and  $\alpha = 0.51$ . The dotted line is  $2.3t^{1/2}$  power law.

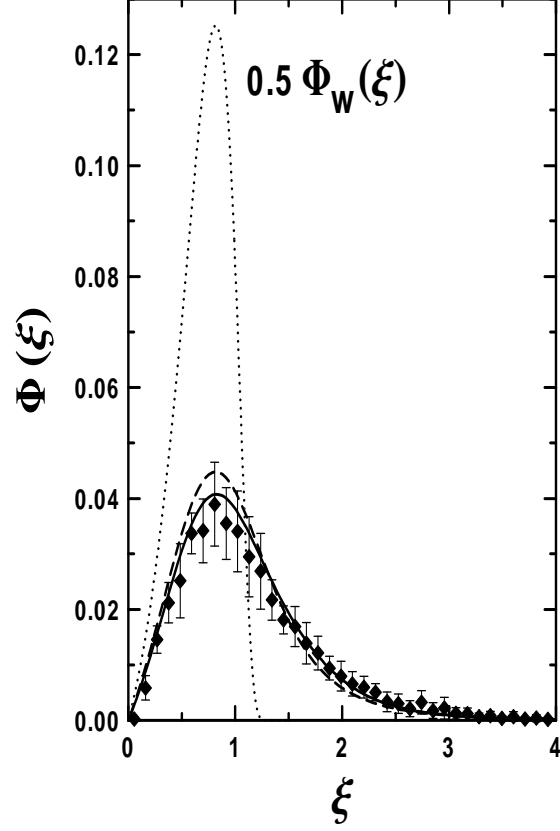


FIG. 6: Scaled distribution function of domain sizes  $\Phi(\xi)$ , where  $\xi = R/t^{1/2}$ . The diamonds represent  $\Phi_{num}(\xi)$ : the scaled distribution obtained in the simulations with the GLE for times  $t > 120$ . The error bars show (twice) the variance of the scaled distribution functions for 13 time moments in the interval  $120 < t < 2900$ . The dotted line is the Wagner distribution  $\Phi_W(\xi)$ , Eq. (14), for the same area fraction  $\varepsilon = 0.25$ . In order to show it on the same graph with  $\Phi_{num}$  we had to multiply it by 0.5. The dashed and solid lines show the distributions  $\Phi_0(\xi)$  and  $\Phi_1(\xi)$ , respectively, predicted by the theory of Ostwald ripening with coalescence, presented in Sec. IV. These distributions represent the zero and first iterations of the iteration procedure [see Sec. IV, Eq. (44)] for  $\beta = 0.93$  which corresponds to  $\varepsilon \simeq 0.25$ .

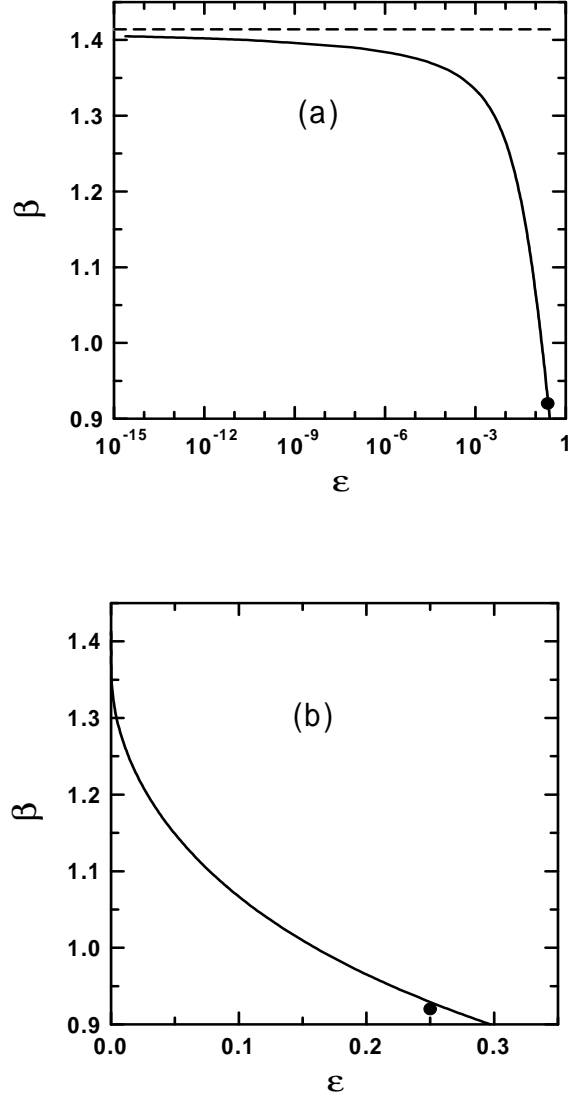


FIG. 7: Parameter  $\beta$  versus  $\varepsilon$  (solid lines) as predicted by the theory of Ostwald ripening with coalescence. This dependence was obtained by a single iteration applied to Eqs. (37) and (31). The dashed line shows the limiting value  $\beta = \sqrt{2}$  expected at  $\varepsilon \rightarrow 0$ . The solid circle is the point found in our phase-field simulations. Figure (a) shows  $\varepsilon$  in a logarithmic scale, figure (b) in a linear scale.